Available online at www.sciencedirect.com
SCIENCE DIRECT®
International Journal of Solids and Structures 42 (2005) 2011–2032
INTERNATIONAL JOURNAL OF SOLIDS and STRUCTURES
www.elsevier.com/locate/ijsolstr

Mode III crack in power law hardening solid

Johannes Weertman *

Department of Materials Science and Engineering, Department of Geological Sciences, Northwestern University, 2220 Campus Drive, Evanston, IL 60208, USA

Received 1 March 2004; received in revised form 26 August 2004
Available online 18 October 2004

Abstract

An approximate solution is obtained for the mode III crack in full scale yielding in a power law work hardening solid. The solution is obtained in stress space. It is based on, and is a modification of, the stress and strain potentials for the mode III crack in an elastic solid.

Keywords: Mode III crack; Stress–strain potentials; Stress–strain spaces; Work hardening

1. Introduction

The only analytic solution that has been obtained for a crack in a power law work hardening solid in general yielding is that of Amazigo (1974, 1975). He obtained, for the mode III crack, a two part solution in strain space for the strain potential using the Wiener–Hopf technique. No attempt was made in this paper to calculate the stress or strain field from the analytical solution except very close to the crack tip. (In Appendix A of this paper we show numerically that the two halves of the Amazigo solution, and their derivatives, do agree at their common border, a demonstration neglected before, if some corrections are made to the solution. Also given in this appendix are corrections to some of the values of the constant that give the values of the J-integral in the first Amazigo paper.)

In the text below is given a more directly developed analytic solution of Amazigo's problem (which, according to his acknowledgment, was suggested to him by J.W. Hutchinson). The solution is an approximate one but its accuracy can be increased at will by increasing the number of terms used. It is found using

* Tel.: +1 847 491 3197; fax: +1 847 467 6573.
E-mail address: j-weertman2@northwestern.edu

0020-7683/$ - see front matter © 2004 Elsevier Ltd. All rights reserved.
doi:10.1016/j.ijsolstr.2004.08.022

the Amazigo approach of working in strain or stress space. This solution, as does Amazigo's, reduces to that of the elastic case. The reason for using stress or strain space is to take advantage of the fact that in these spaces potential functions that give rise to stress and strain fields that satisfy the power law work hardening constitutive law are additive. In real space they are not.

The power law constitutive law, with power exponent in the range $0 \leqslant m \leqslant 1$, considered here is

$$\sigma = \sigma_0 \left(\frac{\epsilon}{\epsilon_0}\right)^m, \quad \frac{\sigma_{yz}}{\sigma_{zx}} = \frac{\epsilon_{yz}}{\epsilon_{zx}}. \tag{1}$$

Here σ_0 and ϵ_0 are (redundant) constants, $\sigma = \sqrt{\sigma_{zx}^2 + \sigma_{yz}^2}$, $\epsilon = \sqrt{\epsilon_{zx}^2 + \epsilon_{yz}^2}$, and σ_{ij} and ϵ_{ij} are the stress and strain components of antiplane strain. The solution sought is for a crack in an infinite medium of half length a that lies on the $y = 0$ plane between $-a \leqslant x \leqslant a$. The solid is stressed at great distance from the crack with an applied stress $\sigma_{yz} = \sigma_A$. (At great distances the strain is $\epsilon_{yz} = \epsilon_A = \epsilon_0 (\sigma_A/\sigma_0)^{1/m}$.) The solution is sought in stress (or strain) space.

In the subsections below a review is given of stress and strain spaces and the equations Amazigo derived that the stress and strain potentials must satisfy in stress and strain space. (Amazigo considered only strain space. However, the change required for stress space is obvious.) In the last subsection a review is presented of the elastic case stress and strain potential solution for the mode III crack. The power law work hardening solution of the text is based on this elastic solution.

1.1. Stress (or strain) space

To enter stress (or strain) space the following interchanges are made (Amazigo, 1974; Appendix G of Weertman, 1996)

$$x \leftrightarrow \varsigma_x \equiv \sigma_{yz}, \quad y \leftrightarrow \varsigma_y \equiv \sigma_{zx},$$

$$x \leftrightarrow \gamma_x \equiv \epsilon_{yz}, \quad y \leftrightarrow \gamma_y \equiv \epsilon_{zx},$$

$$a \leftrightarrow \varsigma_A \equiv \sigma_A, \quad a \leftrightarrow \gamma_A \equiv \epsilon_A, \quad G \leftrightarrow b,$$

$$\theta \equiv \tan^{-1}(y/x) \leftrightarrow \phi \equiv \tan^{-1}(\varsigma_y/\varsigma_x) = \tan^{-1}(\gamma_y/\gamma_x),$$

$$r \leftrightarrow \sigma, \quad r \leftrightarrow \gamma,$$

$$x_r \equiv x\cos\phi - y\sin\phi \leftrightarrow \varsigma_r \equiv \sigma_{\theta z}, \quad x_\theta \equiv x\sin\phi + y\cos\phi \leftrightarrow \varsigma_\theta \equiv \sigma_{zr},$$

$$x_r \equiv x\cos\phi - y\sin\phi \leftrightarrow \gamma_r \equiv \epsilon_{\theta z}, \quad x_\theta \equiv x\sin\phi + y\cos\phi \leftrightarrow \gamma_\theta \equiv \epsilon_{zr},$$

The equivalent of the Burgers vector in stress space is the shear modulus G and b, the Burgers vector, represents the shear modulus in this space. The notation is that in Weertman (1996). (In Amazigo's paper our γ_x and γ_y (and ς_x and ς_y) appear as γ_y and γ_x (and τ_y and τ_x) and our ϕ as $-\phi$. That paper is developed in strain space whereas ours is done in stress space.) The x_r and x_θ cylindrical coordinate relationships here and in the equations below are implicit in the above references. (Note, for example, that $\sigma_{\theta z} = \sigma_{yz}\cos\theta - \sigma_{zx}\sin\theta$.)

Figs. 1 and 2 show how right side positions about a crack (indicated as a horizontal line) in real space map into stress space. The circle represent distant points from the crack. (Strain space is obtained by replacing ς_x with ϵ_x and ς_y with ϵ_y in Fig. 2.) A point b immediately above the crack in real space is mapped below the stress space crack on the vertical ς_y axis. A distant point $\underline{2}$ below the plane of the crack in real space is mapped to the crack tip, above the plane of the stress space crack, in stress space.

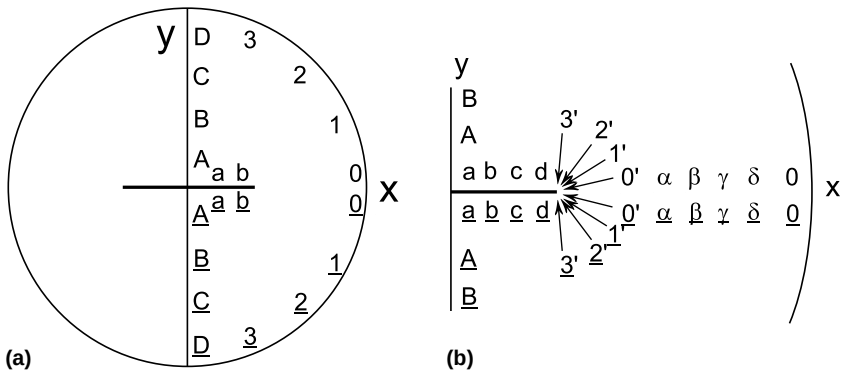

Fig. 1. (a) Crack in real space. (b) Close up of crack region in real space.

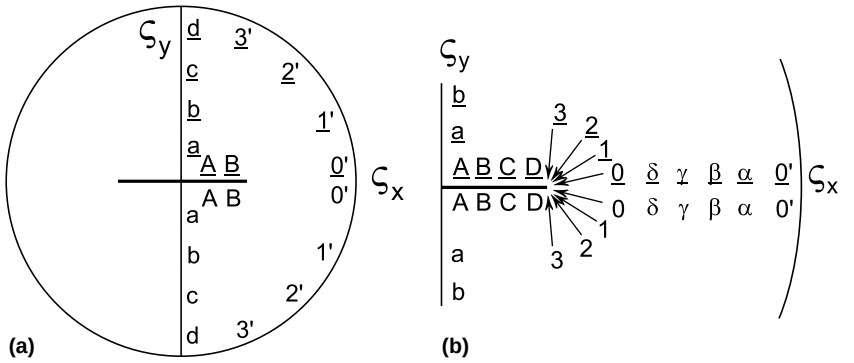

Fig. 2. (a) Crack in stress space. (b) Close up of crack region in stress space.

The equilibrium and strain compatibility equations in antiplane strain are

$$\frac{\partial \varsigma_y}{\partial x}+\frac{\partial \varsigma_x}{\partial y}=0, \quad \frac{\partial \gamma_x}{\partial x}-\frac{\partial \gamma_y}{\partial y}=0. \tag{2}$$

These equations inverted to (Amazigo, 1974; Weertman, 1996)

$$\frac{\partial x}{\partial \varsigma_y}+\frac{\partial y}{\partial \varsigma_x}=0, \quad \frac{\partial x}{\partial \gamma_x}-\frac{\partial y}{\partial \gamma_y}=0. \tag{3}$$

In cylindrical coordinates these equations become

$$\frac{\partial \varsigma_\theta}{\partial r}+\frac{\varsigma_\theta}{r}+\frac{\partial \varsigma_r}{r\partial \theta}=0, \quad \frac{\partial \gamma_r}{\partial r}+\frac{\gamma_r}{r}-\frac{\partial \gamma_\theta}{r\partial \theta}=0, \tag{4}$$

$$\frac{\partial x_\theta}{\partial \varsigma}+\frac{x_\theta}{\varsigma}+\frac{\partial x_r}{\varsigma\partial \phi}=0, \quad \frac{\partial x_r}{\partial \gamma}+\frac{\partial x_r}{\gamma}-\frac{\partial x_\theta}{\gamma\partial \phi}=0. \tag{5}$$

Since $\partial/\partial\varsigma=(\partial\gamma/\partial\varsigma)\partial/\partial\gamma=(\gamma/m\varsigma)\partial/\partial\gamma$ and $\partial/\partial\gamma=(\partial\varsigma/\partial\gamma)\partial/\partial\varsigma=(m\varsigma/\gamma)\partial/\partial\varsigma$, Eq. (5) can be expressed as

$$\frac{1}{m}\frac{\partial x_\theta}{\partial \gamma}+\frac{x_\theta}{\gamma}+\frac{\partial x_r}{\gamma\partial \phi}=0, \quad m\frac{\partial x_r}{\partial \varsigma}+\frac{\partial x_r}{\varsigma}-\frac{\partial x_\theta}{\varsigma\partial \phi}=0. \tag{6}$$

1.2. Stress and strain potentials

In real space the stress components and the strain components are given by the derivatives of the stress and strain potentials u and v:

$$\varsigma_x = \frac{\partial u}{\partial x}, \quad \varsigma_y = -\frac{\partial u}{\partial y}, \quad \gamma_x = \frac{\partial v}{\partial y}, \quad \gamma_y = \frac{\partial v}{\partial x}, \tag{7}$$

$$\varsigma_r = \frac{\partial u}{\partial r}, \quad \varsigma_\theta = -\frac{\partial u}{r\partial\theta}, \quad \gamma_r = \frac{\partial v}{r\partial\theta}, \quad \gamma_\theta = \frac{\partial v}{\partial r}. \tag{8}$$

(v, of course, is the displacement in the z-direction.) Let $\overline{u}$ be the stress space equivalent of the stress potential of real space and $\overline{v}$ the strain space equivalent of the strain potential of real space. Eqs. (7) and (8) in stress and in strain space become

$$x = \frac{\partial \overline{u}}{\partial \varsigma_x}, \quad y = -\frac{\partial \overline{u}}{\partial \varsigma_y}, \quad x = \frac{\partial \overline{v}}{\partial \gamma_y}, \quad y = \frac{\partial \overline{v}}{\partial \gamma_x}, \tag{9}$$

$$x_r = \frac{\partial \overline{u}}{\partial \varsigma}, \quad x_\theta = -\frac{\partial \overline{u}}{\varsigma\partial\phi}, \quad x_r = \frac{\partial \overline{v}}{\gamma\partial\phi}, \quad x_\theta = \frac{\partial \overline{v}}{\partial \gamma}. \tag{10}$$

Eqs. (6) and (10) combine to give Amazigo's equations (for stress space)

$$\frac{\partial^2 \overline{u}}{\partial \varsigma^2} + \frac{1}{m\varsigma}\frac{\partial \overline{u}}{\partial \varsigma} + \frac{1}{m\varsigma^2}\frac{\partial^2 \overline{u}}{\partial \phi^2} = 0, \tag{11}$$

and (for strain space)

$$\frac{\partial^2 \overline{v}}{\partial \gamma^2} + \frac{m}{\gamma}\frac{\partial \overline{v}}{\partial \gamma} + \frac{m}{\gamma^2}\frac{\partial^2 \overline{v}}{\partial \phi^2} = 0 \tag{12}$$

1.3. Elastic case solution

For the elastic case, because $m = 1$, the stress and strain potentials $\overline{u}$ and $\overline{v}$ have the identical form of u and v in real space. In real space (Weertman, 2000, 2001)

$$u^2 = \tfrac{1}{2}\varsigma_A^2\left\{r^2\cos 2\theta - a^2 + \sqrt{r^4 - 2r^2a^2\cos 2\theta + a^4}\right\}, \tag{13}$$

$$v^2 = \tfrac{1}{2}\gamma_A^2\left\{-r^2\cos 2\theta + a^2 + \sqrt{r^4 - 2r^2a^2\cos 2\theta + a^4}\right\}. \tag{14}$$

Fig. 3 shows a plot of constant (normalized) stress potential u and (normalized) strain potential v in real space. (In this figure the solid lines of constant v are the finger trajectories across which the shear stress is a maximum and dashed lines of constant u are the thumb trajectories across which the shear stress is a zero.) The stress and strain fields in real space can be found from Eqs. (13) and (14). The stress and strain fields so found are those of the mode III crack in an elastic solid (given, for example, in Chapter 1 of Weertman, 1996). The stress faces are traction free and the stress field at large distances from the crack reduces to $\varsigma_x = \varsigma_A$, $\varsigma_y = 0$. Fig. 4 presents contours of constant stress magnitude in real space (see Appendix B). In stress space (or strain space) the stress magnitude contours are half circles of varying radii centered at the origin.

The stress and strain potentials $\overline{u}$ and $\overline{v}$ in stress and strain space for the crack in an elastic solid, from Eqs. (13) and (14), are

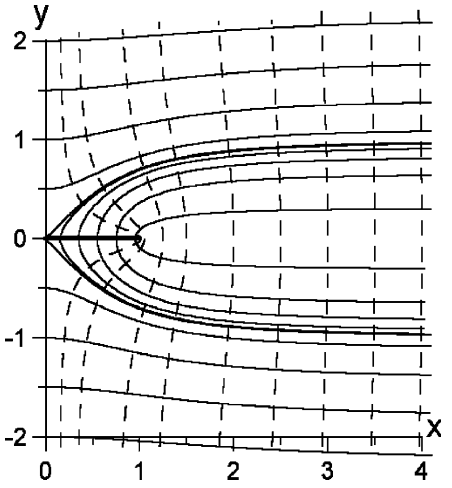

Fig. 3. *Dashed lines*: $u =$ constant. *Solid lines*: $v =$ constant. Right side of mode III crack is shown. Normalized plot.

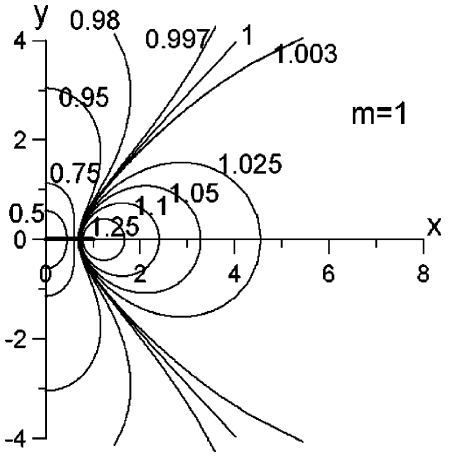

Fig. 4. Stress magnitude contours for mode III crack in elastic solid. Normalized plot.

$$\overline{u}^2 = \tfrac{1}{2}a^2\left\{\varsigma^2\cos 2\phi - \varsigma_A^2 + \sqrt{\varsigma^4 - 2\varsigma^2\varsigma_A^2\cos 2\phi + \varsigma_A^4}\right\}, \tag{15}$$

$$\overline{v}^2 = \tfrac{1}{2}a^2\left\{-\gamma^2\cos 2\phi + \gamma_A^2 + \sqrt{\gamma^4 - 2\gamma^2\gamma_A^2\cos 2\phi + \gamma_A^4}\right\}. \tag{16}$$

The potentials $\overline{u}$ and $\overline{v}$ can be expanded in power series. For ς/ς_A, $\gamma/\gamma_A > 1$,

$$\overline{u}^{>} = a\varsigma_A\left(\frac{\varsigma}{\varsigma_A}\right)\cos\phi - a\varsigma_A\sum_{N=0}^{\infty}a_{2N+1}\left(\frac{\varsigma_A}{\varsigma}\right)^{2N+1}\cos(2N+1)\phi, \tag{17}$$

$$\overline{v}^{>} = a\gamma_A\left(\frac{\gamma}{\gamma_A}\right)\sin\phi + a\gamma_A\sum_{N=0}^{\infty}a^*_{2N+1}\left(\frac{\gamma_A}{\gamma}\right)^{2N+1}\sin(2N+1)\phi. \tag{18}$$

For ς/ς_A, $\gamma/\gamma_A < 1$ (with + for $\phi > 0$ and − for $\phi < 0$)

$$\overline{u}^{<} = \pm\left\{ a\varsigma_A \sum_{N=1}^{\infty} b_{2N} \left(\frac{\varsigma}{\varsigma_A}\right)^{2N} \sin(2N)\phi \right\}, \tag{19}$$

$$\overline{v}^{<} = \pm a\gamma_A \left\{ 1 - \sum_{N=1}^{\infty} b^*_{2N} \left(\frac{\gamma}{\gamma_A}\right)^{2N} \cos(2N)\phi \right\}. \tag{20}$$

The superscript $>$ is used when $\varsigma \geqslant \varsigma_A$ (or $\gamma \geqslant \gamma_A$) and $<$ when $\varsigma \leqslant \varsigma_A$ (or $\gamma \leqslant \gamma_A$). In these equations $a_{2N-1} = a^*_{2N-1} = b_{2N} = b^*_{2N}$ and

$$a_1 = \frac{1}{2}, a_3 = \frac{1\cdot 1}{2\cdot 4}, a_5 = \frac{1\cdot 1\cdot 3}{2\cdot 4\cdot 6}, \ldots, a_{2N+1} = \frac{1\cdot 1\cdot 3\cdot 5\cdots(2N-1)}{2\cdot 4\cdot 6\cdot 8\cdots(2N+2)}. \tag{21}$$

The first three, four and more terms in these equations can be established directly by Taylor expansions of Eqs. (14) and (15). The higher order terms in the equations for $\overline{u}$ can be verified by evaluating the integral

$$\int_0^{\pi} \overline{u}_{\varsigma=\varsigma_A} \{\sin(2N)\phi, \cos(2N+1)\phi\}\, \mathrm{d}\phi,$$

where $\overline{u}$ is given by Eq. (15) and then when $\overline{u}$ is given by Eqs. (17) and (19). The terms in Eqs. (18) and (20) can be verified in the same way. (Note that the constants are the same as those found in the series expansion of the function $\sqrt{1-x}$.)

The following relationships are found connecting a_{2N+1} and b_{2N} by setting $\varsigma = \varsigma_A$, multiplying the right sides of Eqs. (17) and (19) with the term $\cos(2N+1)\theta\,\mathrm{d}\theta$, and integrating from 0 to π (on allowing continuation of $\overline{u}$ into values of ϕ greater than $\pi/2$):

$$a_{2N+1} = -\frac{4}{\pi} \sum_{M=1}^{\infty} b_{2M} \frac{(2M)}{(2M)^2 - (2N+1)^2}, \tag{22}$$

$$a_1 = 1 - \frac{4}{\pi} \sum_{M=1}^{\infty} b_{2M} \frac{(2M)}{(2M)^2 - 1}. \tag{23}$$

The inverse relationship, obtained by using $\sin(2N)\theta\,\mathrm{d}\theta$ instead of $\cos(2N+1)\theta\,\mathrm{d}\theta$, is

$$b_{2N} = \frac{4}{\pi} \frac{(2N)}{(2N)^2 - 1} - \frac{4}{\pi} \sum_{M=0}^{\infty} a_{2M+1} \frac{(2N)}{(2N)^2 - (2M+1)^2}. \tag{24}$$

A numerical evaluation shows that the values of the constants a_{2N+1} and b_{2N} given by Eq. (21) satisfy Eqs. (22)–(24) (as well as Eqs. (27)–(29)).

If Eqs. (17) and (19) are differentiated with respect to ς and then integrated from 0 to ϕ with respect to ϕ (where $\phi \geqslant 0$) the following equations are found:

$$\int_0^{\phi} \varsigma_A \frac{\partial \overline{u}^{>}}{\partial \varsigma}\, \mathrm{d}\phi = a\varsigma_A \left(\frac{\varsigma}{\varsigma_A}\right) \sin\phi + a\varsigma_A \sum_{N=0}^{\infty} a_{2N+1} \left(\frac{\varsigma_A}{\varsigma}\right)^{2N+1} \sin(2N+1)\phi, \tag{25}$$

$$\int_0^{\phi} \varsigma_A \frac{\partial \overline{u}^{<}}{\partial \varsigma}\, \mathrm{d}\phi = a\varsigma_A \left\{ 1 - \sum_{N=1}^{\infty} b_{2N} \left(\frac{\varsigma}{\varsigma_A}\right)^{2N} \cos(2N)\phi \right\}. \tag{26}$$

Note that $\sum_{N=1}^{\infty} b_{2N} = \sum_{N=1}^{\infty} a_{2N+1} = 1$ (a result easily shown from the $x \to 1$ limit of the expansion of $\sqrt{1-x}$). Eqs. (25) and (26) are of the same form as the strain potentials (18) and (20). In the same way that

Eqs. (22)–(24) are obtained from Eqs. (17) and (19) the following equations are obtained from the last two equations:

$$a_{2N+1} = \frac{4}{\pi}\frac{1}{(2N+1)} - \frac{4}{\pi}\sum_{M=1}^{\infty} b_{2M}\frac{(2N+1)}{(2N+1)^2-(2M)^2}, \tag{27}$$

$$a_1 = -1 + \frac{4}{\pi} - \frac{4}{\pi}\sum_{M=1}^{\infty} b_{2M}\frac{1}{1-(2M)^2}, \tag{28}$$

$$b_{2N} = -\frac{4}{\pi}\frac{1}{1-(2N)^2} - \frac{4}{\pi}\sum_{M=0}^{\infty} a_{2M+1}\frac{(2M+1)}{(2M+1)^2-(2N)^2}. \tag{29}$$

2. Mode III crack solution in work hardening solid in stress space

When $m = 1$ the various terms, such as $(\varsigma_A/\varsigma)^{2N+1}\cos(2N+1)\phi$, in Eqs. (17)–(20) obviously satisfy the Amazigo Eqs. (11) and (12). When $m \neq 1$ the exponents over terms such as (ς/ς_A) must change value if these terms are to satisfy Eqs. (11) and (12). The Amazigo equations require the exponent $2N+1$ over a $\frac{\varsigma_A}{\varsigma}$ term or a $\frac{\gamma_A}{\gamma}$ term is replaced with the exponents (Amazigo, 1974)

$$\alpha_{\varsigma(2N+1)} = \frac{1}{2}\left[-\left(1-\frac{1}{m}\right) + \sqrt{\left(1-\frac{1}{m}\right)^2 + \frac{4}{m}(2N+1)^2}\right], \tag{30}$$

$$\alpha_{\gamma(2N+1)} = \frac{1}{2}\left[-(1-m) + \sqrt{(1-m)^2 + 4m(2N+1)^2}\right], \tag{31}$$

where the subscript ς or γ refers to the stress or strain space case. The exponent $2N$ over a $\frac{\varsigma}{\varsigma_A}$ term or a $\frac{\gamma}{\gamma_A}$ term must be replaced with

$$\alpha_{\varsigma(2N)} = \frac{1}{2}\left[\left(1-\frac{1}{m}\right) + \sqrt{\left(1-\frac{1}{m}\right)^2 + \frac{4}{m}(2N)^2}\right], \tag{32}$$

$$\alpha_{\gamma(2N)} = \frac{1}{2}\left[(1-m) + \sqrt{(1-m)^2 + 4m(2N)^2}\right]. \tag{33}$$

This exponent replacement is a necessary condition but is not a sufficient condition for the attainment of a satisfactory solution. The constants a_{2N+1}, b_{2N}, a^*_{2N+1}, b^*_{2N} must also be changed. Their determination is the heart of the problem of the mode III crack in general yielding in a power law work hardening solid. (The arguments of the sin and cosine terms (for example, changing $2N\theta$ to $2\eta\theta$ where η is not an integer) cannot be changed without violating the symmetry conditions—which are the same for the work hardening case as for the elastic case—of the problem.)

2.1. Stress space

In stress space Eqs. (17) and (19) become (for $\varsigma \geqslant \varsigma_A$)

$$\overline{u}^{>} = a\varsigma_A\left(\frac{\varsigma}{\varsigma_A}\right)\cos\phi - a\varsigma_A\sum_{N=0}^{\infty}\overline{a}_{2N+1}\left(\frac{\varsigma_A}{\varsigma}\right)^{\alpha_{2N+1}}\cos(2N+1)\phi, \tag{34}$$

and (for $\varsigma \leqslant \varsigma_A$)

$$\overline{u}^{<} = \pm\left\{ a\varsigma_A \sum_{N=1}^{\infty} \overline{b}_{2N} \left(\frac{\varsigma}{\varsigma_A}\right)^{\alpha_{2N}} \sin(2N)\phi \right\}. \tag{35}$$

New constants $\overline{a}_{2N+1}$ and $\overline{b}_{2N}$ have been substituted for a_{2N+1} and b_{2N}. The subscript ς has been dropped, for simplicity, from the exponents $\alpha_{\varsigma(2N+1)}$ and $\alpha_{\varsigma(2N)}$ of Eqs. (30) and (32).

At $\varsigma = \varsigma_A$ the potential $\overline{u}$ must be continuous (that is, $\overline{u}^{>} = \overline{u}^{<}$). If it were not, infinitely large stresses exist at this circular boundary. (In the elastic case it is obvious that $\overline{u}^{>} = \overline{u}^{<}$ at $\varsigma = \varsigma_A$ because $\overline{u}^{>}$ and $\overline{u}^{<}$ are obtained from Eq. (15) function $\overline{u}$ which is a continuous function at $\varsigma = \varsigma_A$.) Moreover, the derivatives of $\overline{u}^{>}$ and $\overline{u}^{<}$ also must be continuous at $\varsigma = \varsigma_A$. For example, the derivative $-\partial\overline{u}/\varsigma\partial\phi$ gives the stress space analogue of traction stress ς_θ across the $\varsigma = \varsigma_A$ boundary that separates the regions $\varsigma \leqslant \varsigma_A$ and $\varsigma \geqslant \varsigma_A$. The traction stress always must be continuous across a boundary. Thus $\partial\overline{u}/\partial\phi$ is continuous at $\varsigma = \varsigma_A$. (A physical argument, of course, is not needed to deduce the continuity of $\partial\overline{u}/\partial\phi$. If $\overline{u}$ is continuous at $\varsigma = \varsigma_A$, obviously, $\partial\overline{u}/\partial\phi, \partial^2\overline{u}/\partial\phi^2, \partial^3\overline{u}/\partial\phi^3, \ldots$ are continuous too at $\varsigma = \varsigma_A$, as well as the integral $\int_0^\phi \overline{u}\,\mathrm{d}\phi$.)

The derivative $\partial\overline{u}/\partial\varsigma$ gives the stress space analogue of the non-traction stress ς_r across the boundary. Physically, of course, the non-traction stress ς_r can make a jump across a boundary. However, if it does a surface screw dislocation distribution (and an analogue surface screw dislocation distribution in stress space) must exist at the boundary (see p. 51 of Weertman, 1996). But the only surface dislocation distribution that exists for the mode III problem is the distribution that exists at the crack faces. (This distribution does produce a jump in the non-traction stress across the crack faces.) Thus $\partial\overline{u}/\partial\varsigma$ too must be continuous at $\varsigma = \varsigma_A$. If both $\partial\overline{u}/\partial\varsigma$ and $\partial\overline{u}/\varsigma\partial\phi$ are continuous at $\varsigma = \varsigma_A$ and if the potential $\overline{u}$ obeys the Amazigo Eq. (11) on both sides of the boundary then, from Eq. (11), all higher derivatives $\partial^2\overline{u}/\partial\varsigma^2, \partial^3\overline{u}/\partial\varsigma^3, \ldots$ also are continuous.

If the second order derivatives of u and $\overline{u}$ are continuous the physical meaning of this continuity is that the areal screw dislocation density $\mathscr{B}$ (or $\overline{\mathscr{B}}$ for the stress space analogue) is continuous too. The areal screw dislocation density in real or stress space is equal to

$$\mathscr{B} = \frac{1}{G}\nabla^2 u, \quad \overline{\mathscr{B}} = \frac{1}{b}\nabla^2\overline{u}.$$

To have a satisfactory solution, therefore, it is necessary and sufficient to have at the circular boundary $\varsigma = \varsigma_A$:

$$\overline{u}^{>} = \overline{u}^{<}, \quad \frac{\partial\overline{u}^{>}}{\partial\varsigma} = \frac{\partial\overline{u}^{<}}{\partial\varsigma}. \tag{36}$$

The first of these conditions is trivial to satisfy but the second is not.

Let the $\partial/\partial\varsigma$ derivative be taken of Eqs. (34) and (35):

$$\varsigma_A \frac{\partial\overline{u}^{>}}{\partial\varsigma} = a\varsigma_A \cos\phi + a\varsigma_A \sum_{N=0}^{\infty} \overline{a}_{2N+1} \left\{ \frac{1}{2}\left[-\left(1-\frac{1}{m}\right) + \sqrt{\left(1-\frac{1}{m}\right)^2 + \frac{4}{m}(2N+1)^2} \right] \right\} \cos(2N+1)\phi, \tag{37}$$

$$\varsigma_A \frac{\partial\overline{u}^{<}}{\partial\varsigma} = \pm\left\{ a\varsigma_A \sum_{N=1}^{\infty} \overline{b}_{2N} \left\{ \frac{1}{2}\left[\left(1-\frac{1}{m}\right) + \sqrt{\left(1-\frac{1}{m}\right)^2 + \frac{4}{m}(2N)^2} \right] \right\} \sin(2N)\phi \right\}. \tag{38}$$

In these equations $\varsigma/\varsigma_A = \varsigma_A/\varsigma = 1$. These equations can be simplified by subtracting from them Eqs. (34) and (35) after the latter equations are multiplied by the factor $\frac{1}{2}\left(1-\frac{1}{m}\right)$. The result is

$$\varsigma_A \frac{\partial \overline{u}^{>}}{\partial \varsigma} - \frac{1}{2}\left(1-\frac{1}{m}\right)\overline{u}^{>} = \frac{1}{2}\left(1+\frac{1}{m}\right)a\varsigma_A \cos\phi + a\varsigma_A \sum_{N=0}^{\infty} \overline{a}_{2N+1}\left\{\frac{1}{2}\sqrt{\left(1-\frac{1}{m}\right)^2 + \frac{4}{m}(2N+1)^2}\right\}\cos(2N+1)\phi, \tag{39}$$

$$\varsigma_A \frac{\partial \overline{u}^{<}}{\partial \varsigma} - \frac{1}{2}\left(1-\frac{1}{m}\right)\overline{u}^{<} = \pm\left\{a\varsigma_A \sum_{N=1}^{\infty} \overline{b}_{2N}\left\{\frac{1}{2}\sqrt{\left(1-\frac{1}{m}\right)^2 + \frac{4}{m}(2N)^2}\right\}\sin(2N)\phi\right\}. \tag{40}$$

These derivatives must be continuous too.

Let Eqs. (39) and (40) be integrated from $\pi/2$ to $\phi \geqslant 0$. This procedure has the advantage that the increase produced by the differentiation by a factor of about $2N$ or $2N+1$ of the larger order terms is offset by a decrease of the same factor. More important, a mathematical difficulty is eliminated. At $\phi = 0$, $\partial\overline{u}/\partial\varsigma \to \infty$ at a finite but vanishingly small distance ahead of the stress space crack tip and $\partial\overline{u}/\partial\varsigma \to 0$ at finite but vanishingly small distance behind this crack tip. (That is, the crack plane is traction free at the crack faces but the traction stress is exceeding large just ahead of the crack tip.) The result is (on setting $\varsigma/\varsigma_A = \varsigma_A/\varsigma = 1$)

$$\Omega^{>} = \sqrt{m}\frac{1}{2}\left(1+\frac{1}{m}\right)a\varsigma_A(\sin\phi - 1) + a\varsigma_A \sum_{N=0}^{\infty} \overline{a}_{2N+1}\sqrt{1+\frac{(1-m)^2}{4m(2N+1)^2}}\left(\sin(2N+1)\phi - \sin(2N+1)\frac{\pi}{2}\right), \tag{41}$$

$$\Omega^{<} = a\varsigma_A \sum_{N=1}^{\infty} \overline{b}_{2N}\sqrt{1+\frac{(1-m)^2}{4m(2N)^2}}\{\cos N\pi - \cos(2N)\phi\}, \tag{42}$$

where

$$\Omega^{>} \equiv \sqrt{m}\int_{\pi/2}^{\phi}\left\{\varsigma_A\frac{\partial\overline{u}^{>}}{\partial\varsigma} - \frac{1}{2}\left(1-\frac{1}{m}\right)\overline{u}^{>}\right\}\mathrm{d}\phi, \quad \Omega^{<} \equiv \sqrt{m}\int_{\pi/2}^{\phi}\left\{\varsigma_A\frac{\partial\overline{u}^{<}}{\partial\varsigma} - \frac{1}{2}\left(1-\frac{1}{m}\right)\overline{u}^{<}\right\}\mathrm{d}\phi. \tag{43}$$

The $\partial/\partial\varsigma$ derivative condition of Eq. (36) condition can be replaced with the following modified $\partial/\partial\varsigma$ derivative condition at $\varsigma = \varsigma_A$.

$$\Omega^{>} = \Omega^{<}. \tag{44}$$

2.2. Stress space solution

A solution that satisfies these equations is found in the following steps. First set $\overline{u}^{>} = \overline{u}_0^{>}$ and $\overline{u}^{<} = \overline{u}_0^{<}$ where $\overline{u}_0^{>}$ and $\overline{u}_0^{<}$ are given by

$$\frac{\overline{u}_0^{>}}{a\varsigma_A} = \left(\frac{\varsigma}{\varsigma_A}\right)\cos\phi + (\beta_0 - 2)a_1\left(\frac{\varsigma_A}{\varsigma}\right)^{\alpha_1}\cos\phi - \beta_0\sum_{N=1}^{\infty} a_{2N+1}\left(\frac{\varsigma_A}{\varsigma}\right)^{\alpha_{2N+1}}\cos(2N+1)\phi, \tag{45}$$

$$\frac{\overline{u}_0^{<}}{a\varsigma_A} = \pm\beta_0\sum_{N=1}^{\infty} b_{2N}\left(\frac{\varsigma}{\varsigma_A}\right)^{\alpha_{2N}}\sin(2N)\phi. \tag{46}$$

Note that $\overline{u}_0^>$ reduces to the correct limit of $a\varsigma\cos\phi$ when $\varsigma \gg \varsigma_A$. Here β_0 is a constant to be set. The constants a_{2N+1} and b_{2N} are those of Eq. (21) of the elastic case. Because they are, setting $\overline{u}^> = \overline{u}_0^>$ and $\overline{u}^< = \overline{u}_0^<$ does satisfy the $\overline{u}^> = \overline{u}^<$ continuity condition at $\varsigma = \varsigma_A$. However, the modified derivative condition $\Omega_0^> = \Omega_0^<$ is not satisfied (on setting $\overline{u}^> = \overline{u}_0^>$, $\overline{u}^< = \overline{u}_0^<$, $\varsigma = \varsigma_A$, $\overline{b}_{2N} = \beta_0 b_{2N}$, $\overline{a}_{2N+1} = \beta_0 a_{2N+1}$, and $\overline{a}_1 = (2-\beta_0)a_1$, in the right-hand side of Eqs. (39)–(42)).

Instead of substituting $\overline{u}_0^>$ and $\overline{u}_0^<$ into Eqs. (39)–(42) substitute

$$\overline{u}_{2K}^< = a\varsigma_A\left(\frac{\varsigma}{\varsigma_A}\right)^{\alpha_{2K}}\sin 2K\phi, \quad \overline{u}_{2K}^> = -a\varsigma_A\sum_{N=0}^{\infty}\widetilde{a}_{2N+1}^{2K}\left(\frac{\varsigma_A}{\varsigma}\right)^{\alpha_{2N+1}}\cos(2N+1)\phi, \tag{47}$$

where $K = 1, 2, 3, \ldots$ and the constants $\widetilde{a}_{2N+1}^{2K}$ are given by

$$\widetilde{a}_{2N+1}^{2K} = -\frac{4}{\pi}\frac{(2K)}{(2K)^2-(2N+1)^2}. \tag{48}$$

Eq. (47) satisfies the $\overline{u}^> = \overline{u}_{2K}^> = \overline{u}^< = \overline{u}_{2K}^<$ continuity condition. It does not satisfy the modified $\partial/\partial\varsigma$ derivative condition (44). The terms $\Omega_{2K}^>(\phi)$ and $\Omega_{2K}^<(\phi)$ are found by setting $\overline{u}^> = \overline{u}_{2K}^>$, $\overline{u}^< = \overline{u}_{2K}^<$, $\varsigma = \varsigma_A$, $\overline{b}_{2N} = 0$ for $N \neq K$, $\overline{b}_{2N} = 1$ for $N = K$, and $\overline{a}_{2N+1} = \widetilde{a}_{2N+1}^{2K}$ in the right-hand side of Eqs. (39)–(42). The term $\frac{1}{2}\left(1+\frac{1}{m}\right)$ in these equations is set equal to zero because it is already accounted for with the potentials $\overline{u}_0^>$ and $\overline{u}_0^<$.

The value of the constant β_0 is set by finding curves $\Delta\Omega_0 = \Omega_0^> - \Omega_0^<$ versus ϕ for different values of β_0. The value of β_0 chosen is that for the curve that, apart from the scaling factor, most closely matches in form the curve of $\Delta\Omega_2 = \Omega_2^> - \Omega_2^<$ versus ϕ. Fig. 5a and b show, for $m = 1/5$ and $m = 1/100$, curves of $\Delta\Omega_0$ versus ϕ for different values of β_0. Also shown in these figures are the dashed curves $-\beta_2\Delta\Omega_2$ versus ϕ where β_2 values are given in Table 1 of Appendix C. The $\Delta\Omega_0$ curves for $\beta_0 = 1.2184$ and $\beta_0 = 2.63$ most closely match the $-\beta_2\Delta\Omega_2$ curves.

Potentials that do satisfy Eq. (44) approximately are found, using a finite number of constants $\beta_2, \beta_4, \beta_6, \ldots, \beta_{2n}$ on setting

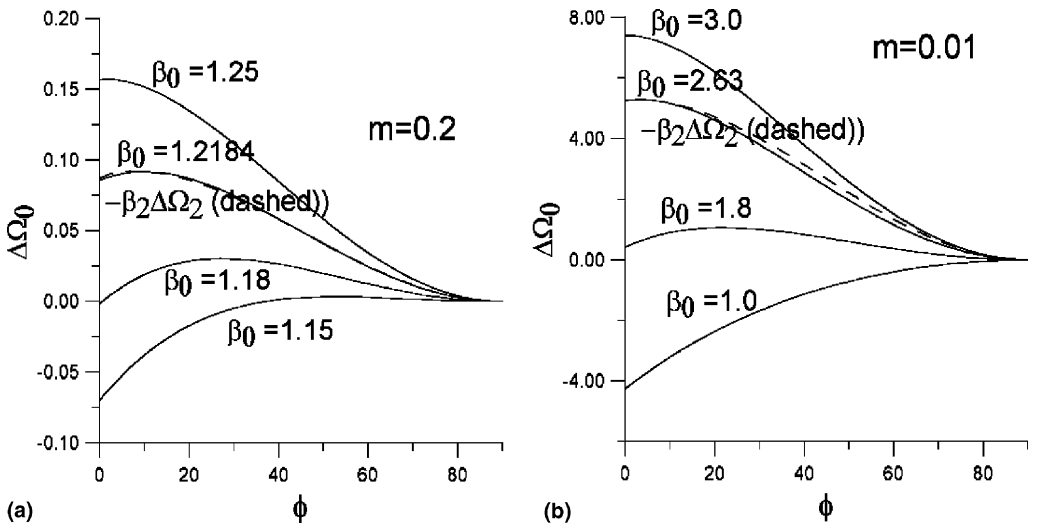

Fig. 5. (a) $\Delta\Omega_0$ versus ϕ for $m = 1/5$. (b) $\Delta\Omega_0$ versus ϕ for $m = 1/100$.

$$\overline{u}^{>} = \overline{u}_0^{>} + \sum_{N=1}^{n} \beta_{2N} \overline{u}_{2N}^{>}, \quad \overline{u}^{<} = \overline{u}_0^{<} + \sum_{N=1}^{n} \beta_{2N} \overline{u}_{2N}^{<}. \tag{49}$$

The constants $\overline{a}_{2N+1}$ and $\overline{b}_{2N}$ are equal to (where $\beta_{2N} = 0$ for $N > n$)

$$\overline{a}_{2N+1} = \beta_0 a_{2N+1} + \sum_{K=1}^{n} \beta_{2K} \widetilde{a}_{2N+1}^{2K}, \quad \overline{b}_{2N} = \beta_0 b_{2N} + \beta_{2N}, \tag{50}$$

$$\overline{a}_1 = (2 - \beta_0) a_1 + \sum_{K=1}^{n} \beta_{2K} \widetilde{a}_1^{2K}. \tag{51}$$

The $\overline{u}^{>} = \overline{u}^{<}$ continuity condition at $\varsigma = \varsigma_A$ remains satisfied by Eq. (49) regardless of the values of the constants β_{2N}. Values of the constants β_{2N} that allow the modified $\partial/\partial\varsigma$ derivative condition (44) to be satisfied approximately are found by setting

$$\Delta\Omega_0(\phi) + \sum_{N=1}^{n} \beta_{2N} \Delta\Omega_{2N}(\phi) = 0, \tag{52}$$

at n different values of the angle ϕ and solving the resultant n independent equations for the n constants β_{2N}. The larger is n the more accurate the solution.

Let the number n be limited to 5. Let the angles used in Eq. (52) be 0°, 18°, 36°, 54°, 72°. In Appendix C are listed values of β_{2N} found from the last equation for a number of values of the power exponent m. In Fig. 6 are plots of $\Omega^{>}$ and $\Omega^{<}$ versus ϕ for three different values of m. Points plotted are calculated at 2.5° intervals. In Appendix C is given a table that lists the values of $\Omega^{>}$ and $\Omega^{<}$ at different values of ϕ for the case of $m = 1/5$. The solutions of Fig. 6 and Appendix C are reasonably accurate. Fig. 7 shows a plot of the essentially unmodified $\partial/\partial\varsigma$ derivative (given by Eqs. (39) and (40)) versus ϕ. (In calculating the curves in Figs. 5–7 summations were taken over 5×10^4 terms except at $\phi = 0°$ when 10^6 terms were used. In Fig. 7 10^6 terms were used when $\phi < 26°$. Summation tricks discussed in Appendix D also were used.)

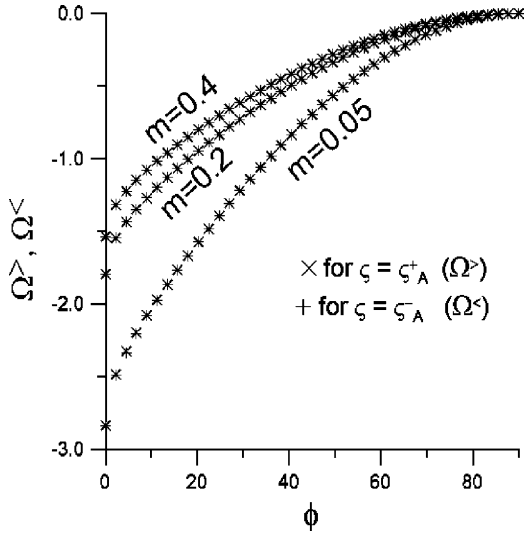

Fig. 6. $\Omega^{>}$ and $\Omega^{<}$ versus ϕ.

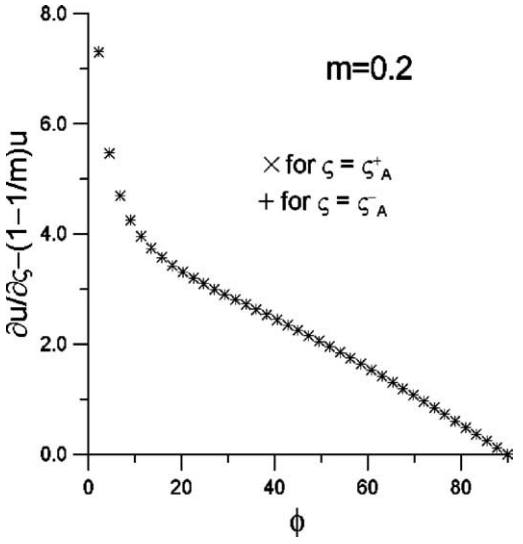

Fig. 7. $\partial u/\partial\varsigma - (1-\frac{1}{m})u$ versus ϕ.

3. Stress magnitude contours in real space

In stress space the real space coordinates are found as a function of ς and ϕ (or ς_x and ς_y). Thus, from Eqs. (9) and (10),

$$x = x_r \cos\phi + x_\theta \sin\phi, \quad y = -x_r \sin\phi + x_\theta \cos\phi, \tag{53}$$

where

$$x_r = \frac{\partial \overline{u}}{\partial \varsigma}, \quad x_\theta = -\frac{\partial \overline{u}}{\varsigma \partial \phi}. \tag{54}$$

For the mode III crack problem $\overline{u}$ is given by Eqs. (45)–(51). Thus given a stress component the real space coordinates associated with it can be found.

The constant stress magnitude contours in real space are easily found from these equations by fixing the value of ς and varying the angle ϕ until the contour is traced out. Fig. 8a–e show stress magnitude contours so found for $m = 2/5$, 1/5, 1/20, 1/40, 1/100. (The case of $m = 1$ is shown in Fig. 4.) These plots are normalized by setting $a = \varsigma_A = 1$.

Fig. 9a–c shows stress magnitude contours close to the crack tip for $m = 1/5$ and $m = 1/40$. (In these figures the origin is at the crack tip.) Fig. 9a and b have the same spatial extent. The non-concentric circles for the $m = 1/5$ case are non-concentric elliptically shaped contours for the $m = 1/40$ case. Fig. 9c shows that closer to the crack tip the contours for the $m = 1/40$ case also are non-concentric circles. (Rice (1968) showed that in small scale yielding in a work hardening solid the stress magnitude contours close to the crack tip are non-concentric circles.)

It is seen in Fig. 8 that the contour found for the (normalized) stress magnitude ς which is slightly larger than one (1.0001) almost coincides, as it should, with the contour which is slightly smaller than one (0.9999).

The term $\overline{a}_1(\varsigma_A/\varsigma)^{\alpha_1}\cos\phi$ in the expression $\overline{u}^{>}$ in stress space determines the asymptotic crack tip stress field in real space. Likewise, the term $\overline{a}_2(\varsigma/\varsigma_A)^{\alpha_2}\sin 2\phi$ in the expression $\overline{u}^{<}$ gives the asymptotic stress field in real space at the center of the crack. (Note that $\overline{a}_2 = \frac{1}{2}\beta_0 + \beta_2$ and $\overline{a}_1 = \frac{1}{2}(2-\beta_0) + \sum_{K=1}^{5}\beta_{2K}\widetilde{a}_1^{2K}$.)

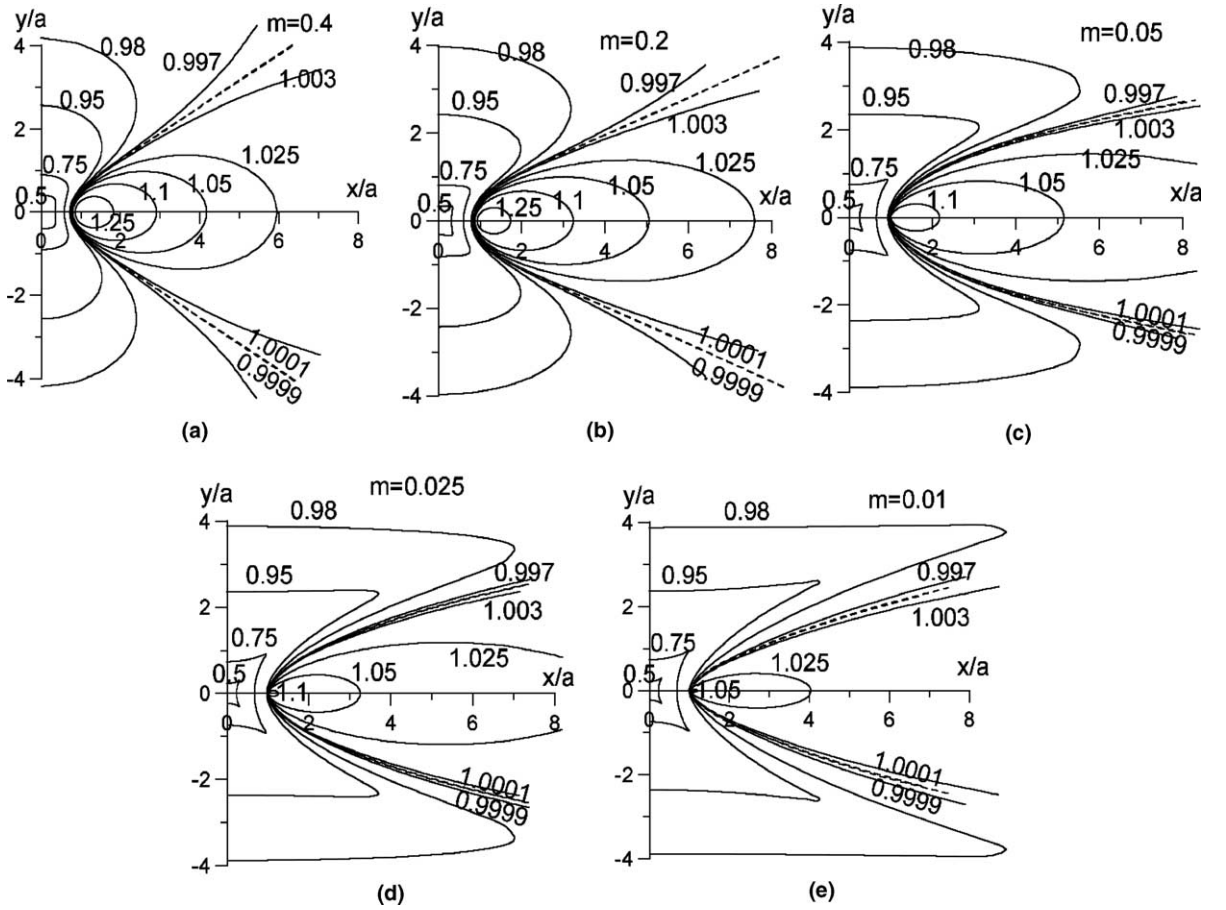

Fig. 8. (a) ς/ς_A contours for $m = 2/5$. (b) ς/ς_A contours for $m = 1/5$. (c) ς/ς_A contours for $m = 1/20$. (d) ς/ς_A contours for $m = 1/40$. (e) ς/ς_A contours for $m = 1/100$.

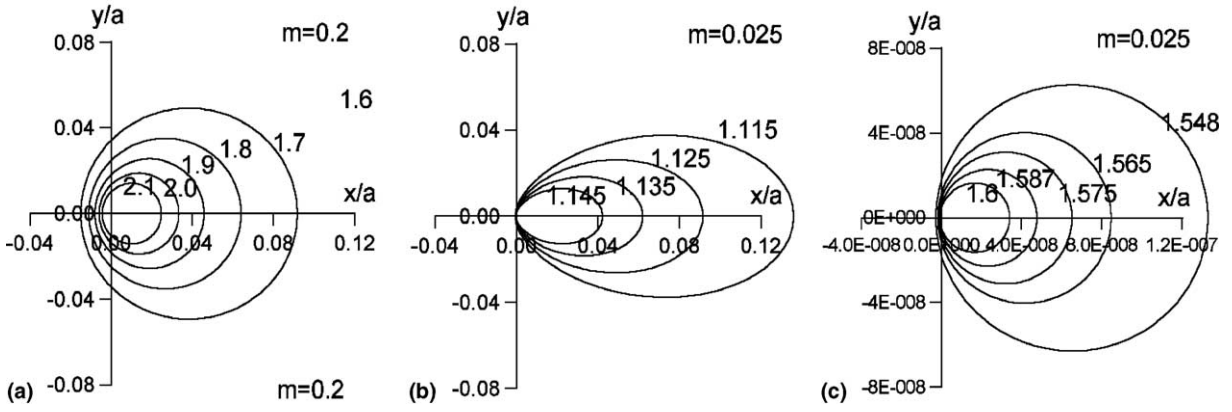

Fig. 9. (a) ς/ς_A contours for $m = 1/5$. (b) ς/ς_A contours for $m = 1/40$. (c) ς/ς_A contours for $m = 1/40$.

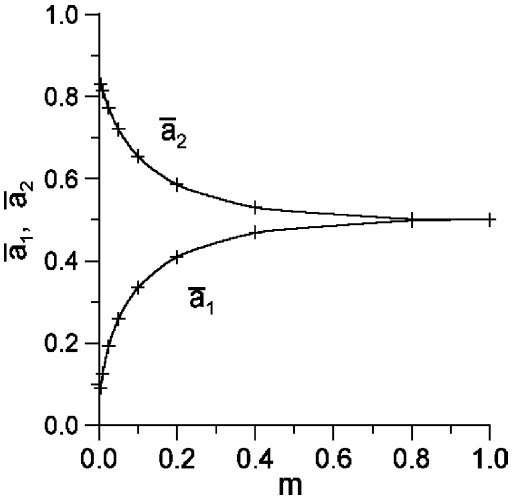

Fig. 10. $\bar{a}_1$ and $\bar{a}_2$ versus m.

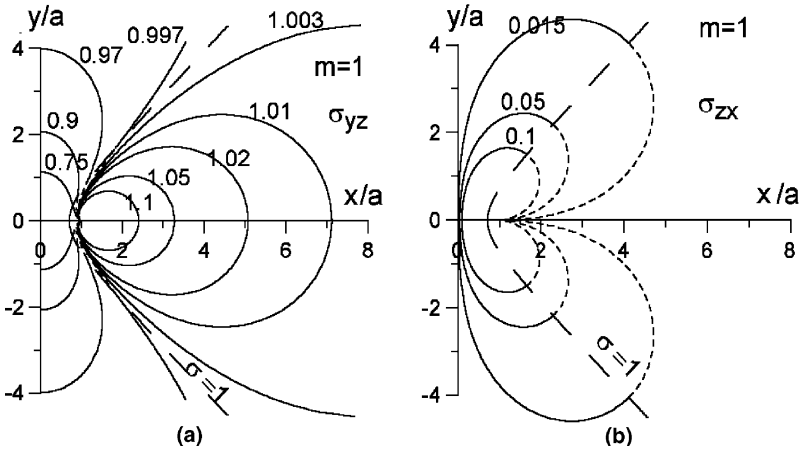

Fig. 11. (a) σ_{yz} contours for $m = 1$. (b) σ_{zx} contours for $m = 1$.

Fig. 10 shows a plot of $\bar{a}_1$ and $\bar{a}_2$ versus m. Table 3 of Appendix C lists values of $\bar{a}_1$ and $\bar{a}_2$ for the different values of m plotted in Fig. 11. It can be seen that the sum $\bar{a}_1 + \bar{a}_2$ is approximately equal to 1. In the limit $m \to 0$ it is likely that $\bar{a}_1 \to 0$ and $\bar{a}_2 \to 1$. The values of $\bar{a}_1$ and $\bar{a}_2$ are relatively insensitive to the exact value chosen for β_0. (If β_0 is altered somewhat the changes in the constants β_{2N} are such that $\bar{a}_1$ and $\bar{a}_2$ remain almost unaltered.)

4. Stress component contours in real space

In this section normalized contour plots, in real space, are given, for $m = 1, 1/5, 1/40$, for the individual stress components $\varsigma_x \equiv \sigma_{yz}$ and $\varsigma_y \equiv \sigma_{zx}$. To find these contours from Eqs. (9), (17) and (19) it is only

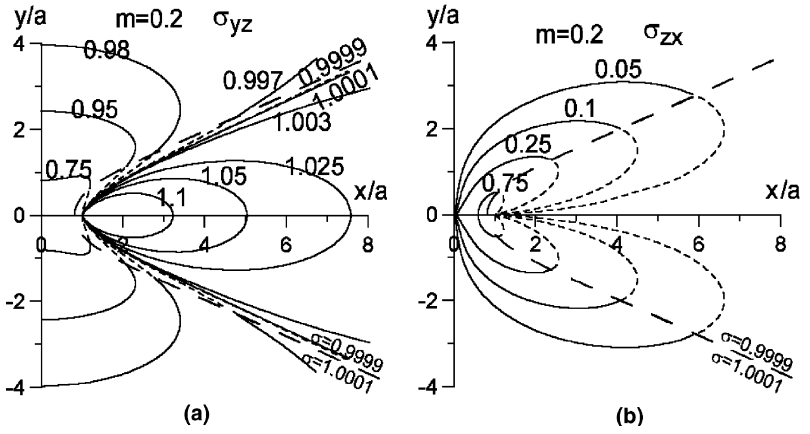

Fig. 12. (a) σ_{yz} contours for $m = 1/5$. (b) σ_{zx} contours for $m = 1/5$.

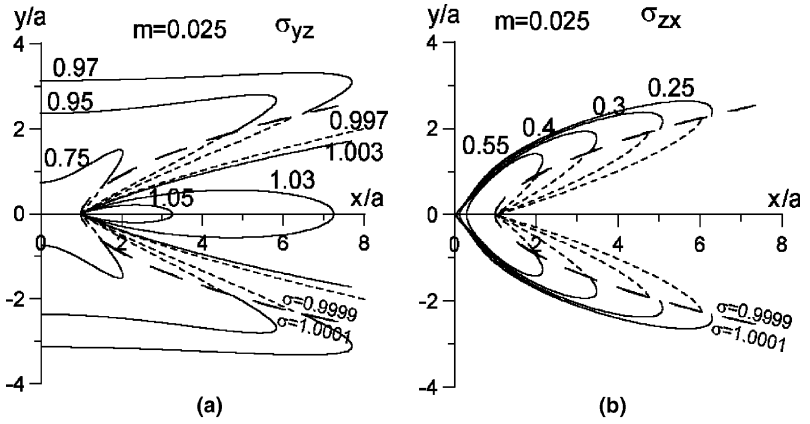

Fig. 13. (a) σ_{yz} contours for $m = 1/40$. (b) σ_{zx} contours for $m = 1/40$.

necessary to set the expression $\varsigma\cos\phi = \varsigma_x$ (or $\varsigma\sin\phi = \varsigma_y$) equal to a constant while varying ς and ϕ. Figs. 11–13 present normalized contour plots of constant $\sigma_{yz} \equiv \varsigma_x$ and constant $|\sigma_{zx}| \equiv |\varsigma_y|$. Also shown in these plots, as long dashed curves, are the constant stress magnitude contour $\sigma = 1.0001\sigma_A \approx \sigma_A$ found for $u = u^{>}$ (Eq. (17)) and the contour $\sigma = 0.9999\sigma_A \approx \sigma_A$ found for $u = u^{<}$ (Eq. (19)). In the plots the stress is normalized by dividing by σ_A and the distance x and y from the crack center is normalized by dividing by the crack half length a. Only the right side of the space around the crack is shown. The sign of σ_{yz} is positive on the right side of the origin and negative on the left. One the right side the sign of σ_{xz} is negative above the crack plane and positive below it.

Eq. (19) is used to find the contours in the region where $\sigma/\sigma_A \equiv \varsigma/\varsigma_A < 1$ (to the left of the $\varsigma/\varsigma_A = 1$ contour) and Eq. (17) where $\sigma/\sigma_A \equiv \varsigma/\varsigma_A > 1$ (to the right of the $\varsigma/\varsigma_A = 1$ contour) In the σ_{zx} contour plots a solid line is used in the regions where $\varsigma/\varsigma_A < 1$ and a dashed line where $\varsigma/\varsigma_A > 1$. For the σ_{yz} plots a solid line is used where $\varsigma/\varsigma_A < 1$. A solid line also is used where $\varsigma/\varsigma_A > 1$ and $\sigma_{yz}/\sigma_A > 1$. A dashed line is used in the region where $\varsigma/\varsigma_A > 1$ but $\sigma_{yz}/\sigma_A < 1$. (Equation (15) was used to find contours for the elastic case of $m = 1$.)

To have a valid solution it is necessary that σ_{yz} and σ_{zx} do not change discontinuously across the constant stress magnitude contour $\sigma = \sigma_A$. On one side of this contour the solution is given by Eq. (17) for $\overline{u}^{>}$. On the other side of the contour the solution is given by Eq. (19) for $\overline{u}^{<}$. The two solutions must match at the $\sigma = \sigma_A$ contour (and the $\sigma \approx \sigma_A$ contours found for $u = u^{>}$ and $u = u^{<}$ must superimpose). This match is excellent in Fig. 12a and b for the $m = 1/5$ case. It is not bad for the case when m has the very small value of $m = 1/40$, shown in Fig. 13a and b. A better match for the $m = 1/40$ example can be obtained by finding additional constants β_{2N} beyond the six listed in Table 1 of Appendix C. The approximate solution of the mode III crack in a power law hardening solid appears to be a reasonable one.

5. Discussion

To have a successful solution it is necessary to show, in stress space, that the derivative $\partial\overline{u}/\partial\varsigma$, or the modified derivative Ω, is continuous at $\varsigma = \varsigma_A$. This continuity to reasonable accuracy (see Figs. 6 and 7 and Table 2) is demonstrated in the analysis of the paper. The solution, as required, does reduce to that of the mode III crack in an elastic solid. It should be possible to repeat the analysis of the paper in strain space to obtain an equivalent solution for the mode III crack. The success of the approximate solution of this paper with use of the constant β_0 and only the five constants β_2, β_4, β_6, β_8, β_{10} arises from the fortunate circumstance that by varying the value of β_0 a $\Delta\Omega_0$ (modified derivative) difference curve can be found that matches closely a scaled $\Delta\Omega_2$ difference curve (see Fig. 5a and b). Without this match the method of this paper would require use of many more β_{2N} terms. From Fig. 5a and b, and data not shown, it is seen that the match becomes poorer the smaller m becomes. To obtain the same accuracy found, in matching the $\partial\overline{u}/\partial\varsigma$ derivative at $\varsigma = \varsigma_A$, with the larger values of m obvious requires use of more than five β_{2N} terms when m is small.

By changing the value of β_0 it is possible to improve the agreement of the $\partial\overline{u}/\partial\varsigma$ derivative at $\varsigma = \varsigma_A$ over the entire angular range of ϕ. But a point is reached when further improvement of the agreement over part of the angular range of ϕ comes at the expense of reducing the agreement over another part of the angular range. There is a small range of values of β_0 that give about equally good approximate solutions. There is no unique value for the β_0 term.

It is to be noted in Figs. 4 and 8 that the position where the constant stress magnitude crosses the y-axis is not much altered on changing m from 1 to a small value. On the crack plane behind the crack tip the $\varsigma/\varsigma_A = 1$ contour crosses the crack plane at $x/a = 1/\sqrt{2} \approx 0.7071$ when $m = 1$ and $x/a \to 1$ as $m \to 0$. The elliptically shaped contours for $\varsigma/\varsigma_A > 1$ initially become longer (and narrower) as m becomes smaller. They then become smaller on further decrease of m and shrink into the crack tip. (A larger stress magnitude contour may be shrinking while a smaller value contour is growing in length as m decreases.)

It should be pointed out that the constitutive law used in the analysis requires the shear modulus be infinitely large to avoid negative unloading strain on stress removal after small deformation (Amazigo, 1974). When the shear modulus is finite the solution should be good almost everywhere except close to the center of the crack. In this region the stress and strain are small. The constitutive equation (1) needs to be altered in this region if the shear modulus is finite. Near the crack tip the solution breaks down because it requires the non-redundant dislocation density ρ_N (geometrically necessary dislocation density) be very much greater than the redundant dislocation density ρ_R (statistically stored dislocation density) (Weertman, 1991, 1996). No likely mechanism evidently exists in the tip region to pin non-redundant dislocations in place. The crack tip region could be, effectively, a region almost free of non-redundant dislocations (that is, ρ_N is reduced to the level of ρ_R) (Thomson, 1978; Weertman, 1978, 1996).

Acknowledgements

Parts of this paper were presented at the symposium held during the TMS 2004 winter meeting to honor Professor Richard Arsenault. Dick was my first Ph.D. student. It was a great pleasure to participate in this symposium held to honor all his remarkable work that started many years ago at Northwestern.

Appendix A

Amazigo's notation is used in this appendix. Note: his normalized ρ corresponds to our γ/γ_A; his power law exponent n and our exponent m are related by $n = 1/m$; the origin in real space is taken at the right side crack tip, rather than at crack center. (This shift of origin causes the $\rho\sin\phi$ term to appear in the potential for $\rho < 1$ rather than in the potential for $\rho > 1$.) When $\rho < 1$ Amazigo's solution (1974) for the potential $\Psi(\rho,\phi)$ in strain space is given by

$$\Psi(\rho,\phi) = -\frac{2}{\pi}\frac{N_{-1}(n,-1)}{N_{-1}(n,0)} + \rho\sin\phi + \frac{1}{\pi}\sum_{m=1}^{\infty}\frac{N_{-1}(n,-1)[1-n(b_m+1)]}{m(1+b_m)N_{-1}(n,b_m)\omega'(b_m)}\rho^{-b_m}\cos 2m\phi. \tag{A.1}$$

Here

$$b_m = \frac{1}{2}\left[\frac{1}{n} - 1 - \sqrt{(\frac{1}{n}-1)^2 + \frac{4(2m)^2}{n}}\right], \quad \omega'(b_m) = \frac{2b_m + n - 1}{2\sqrt{b_m(b_m n + n - 1)}},$$

and

$$N_{-1}(n,s) = 2^{-s\sqrt{n}}\frac{\prod_{k=1}^{\infty}(\gamma_{2k-1}^{+} - a_{2k-1}s)\exp(a_{2k-1}\overline{s})}{\prod_{k=1}^{\infty}(\gamma_{2k}^{+} - a_{2k}s)\exp(a_{2k}\overline{s})}, \tag{A.2}$$

where $\gamma_{2k-1}^{+} = \frac{\sqrt{n}}{2(2k-1)}\left[\frac{1}{n} - 1 + \sqrt{(\frac{1}{n}-1)^2 + \frac{4(2k-1)^2}{n}}\right]$, $a_{2k-1} = \frac{\sqrt{n}}{(2k-1)}$, $\overline{s} = s + \frac{1}{2}(1-\frac{1}{n})$, $a_{2k-1} = \frac{\sqrt{n}}{(2k-1)}$, $a_{2k} = \frac{\sqrt{n}}{(2k)}$, etc.

When $\rho > 1$ the potential is

$$\Psi(\rho,\phi) = \frac{1}{\pi}\sum_{m=1}^{\infty}\frac{2^{\sqrt{n}C_m}N_{-1}(n,-1)[1-n(C_m+1)]\prod_{k=1}^{\infty}(\gamma_{2k}^{+} - a_{2k}C_m)\exp(a_{2k}\overline{C}_m)}{\sqrt{n}(1+C_m)\exp\frac{\sqrt{n}\overline{C}_m}{(2m-1)}\prod_{\substack{k=1\\k\neq m}}^{\infty}(\gamma_{2k-1}^{+} - a_{2k-1}C_m)\exp(a_{2k-1}\overline{C}_m)}\rho^{-C_m}\sin(2m-1)\phi, \tag{A.3}$$

where $C_m = \frac{1}{2}\left[\frac{1}{n} - 1 + \sqrt{(\frac{1}{n}-1)^2 + \frac{4(2m-1)^2}{n}}\right]$, $\overline{C}_m = .C_m + \frac{1}{2}(1-\frac{1}{n})$. The corrections have been made in the above equations of $b_m = 2m\gamma_{2m}^{-}/\sqrt{n}$ instead of $b_m = 2m\gamma_m^{-}/\sqrt{n}$ and $\sin(2m-1)\phi$ instead of $\sin(2m+1)\phi$. In addition, the correction factor $\exp[\sqrt{n}\overline{C}_m/(2m-1)]$, has been added. (In Amazigo (1975) it is pointed out that for the $m = 1$ coefficient of Eq. (A.3) a correction factor of $\exp[(n+1)/2\sqrt{n}]$ is required. If, in Eq. (38) of that paper, the term $\exp[\sqrt{n}a_m^{-}/(2n+1)]$ is changed to $\exp[\sqrt{n}\overline{a}_m/(2m+1)]$, then the correction factor $\exp[\sqrt{n}\overline{C}_m/(2m-1)]$ is obtained for Eq. (A.3).)

In the elastic limit these equations reduce to

$$\Psi(\rho,\phi) = -1 + \rho\sin\phi + \frac{2}{\pi}\sum_{m=1}^{\infty}\frac{N_{-1}(n,-1)}{(2m-1)N_{-1}(n,-2m)}\rho^{2m}\cos 2m\phi \tag{A.4}$$

for $\rho < 1$ and, for $\rho > 1$,

$$\Psi(\rho,\phi) = \frac{1}{\pi}\sum_{m=1}^{\infty} \frac{2^{2m-1}(1-2m)N_{-1}(n,-1)\prod_{k=1}^{\infty}\left(1-\frac{2m-1}{2k}\right)\exp\left(\frac{2m-1}{2k}\right)}{(2m)e\prod_{\substack{k=1\\k\neq m}}^{\infty}\left(1-\frac{2m-1}{2k-1}\right)\exp\left(\frac{2m-1}{2k-1}\right)}\rho^{-(2m-1)}\sin(2m-1)\phi. \tag{A.5}$$

Here

$$N_{-1}(n,s) = 2^{-s}\frac{\prod_{k=1}^{\infty}\left(1-\frac{s}{2k-1}\right)\exp\left(\frac{s}{2k-1}\right)}{\prod_{k=1}^{\infty}\left(1-\frac{s}{2k}\right)\exp\left(\frac{s}{2k}\right)}. \tag{A.6}$$

In the elastic solution of the text the coefficients of the trigonometric terms (using m for N) are $b^*_{2m} = a^*_{2m+1} = \frac{1\cdot1\cdot3\cdot5\cdots(2m-1)}{2\cdot4\cdot6\cdot8\cdots(2m+2)}$. These can be expressed as

$$b^*_{2m} = a^*_{2m+1} = \frac{1}{2\sqrt{\pi}}\frac{\Gamma(m+\frac{1}{2})}{\Gamma(m+2)} = \frac{e^{\frac{3}{2}C_E}}{2\sqrt{\pi}}\left(\frac{2m+4}{2m+1}\right)\frac{\prod_{k=1}^{\infty}\left(1+\frac{2m+4}{2k}\right)\exp\left(-\frac{2m+4}{2k}\right)}{\prod_{k=1}^{\infty}\left(1+\frac{2m+1}{2k}\right)\exp\left(-\frac{2m+1}{2k}\right)}. \tag{A.7}$$

Here Γ is the Gamma function and $C_E \approx 0.5772157$ is Euler's constant.

The trigonometric coefficients in either Eq. (A.4) or Eq. (A.5) are of quite different mathematical form from those of Eq. (A.7). However, a numerical evaluation of the coefficients of Eqs. (A.4) and (A.5) (as well as those of Eqs. (A.1) and (A.3) with n set to $n = 1$) reveals that these coefficients are identical to those of Eqs. (21) and (A.7). (We have ignored a difference in sign of between the coefficients. The potential function of Amazigo evidently is the negative of the one in the text as a consequence of the shift of the origin in real space to the crack tip.)

When $\rho = 1$ the potential $\Psi(1, \phi)$, for $\rho \leqslant 1$, found from Eq. (A.1) must equal the potential $\Psi(1, \phi)$, for $\rho \geqslant 1$, found from Eq. (A.3). Fig. 14 shows a plot calculated from these potentials (when $\rho = 1$) as a function of ϕ for $n = 6$. Also plotted in this figure is the function $\int \Psi' \equiv \int_{\pi/2}^{\phi}(\partial\Psi/\partial\rho)\,d\phi$. For a satisfactory solution the Ψ curves should coincide and the $\int\Psi'$ curves also should coincide. It is seen in Fig. 14 that the curves coincide.

Amazigo represents the first summation term of Eq. (A.3) as $Q(n)\rho^{-1/n}\sin\phi$. From his Table 1, which lists values of the J-integral for various values of n, the value of the first summation coefficient Q he calculated can be obtained for a number of values of n. (The coefficient Q has a negative sign.) These are listed as $|Q_{\text{Amaz}}|$ in Table 4 of Appendix C. Also listed in this table are the values we calculated (listed as $|Q|$) from

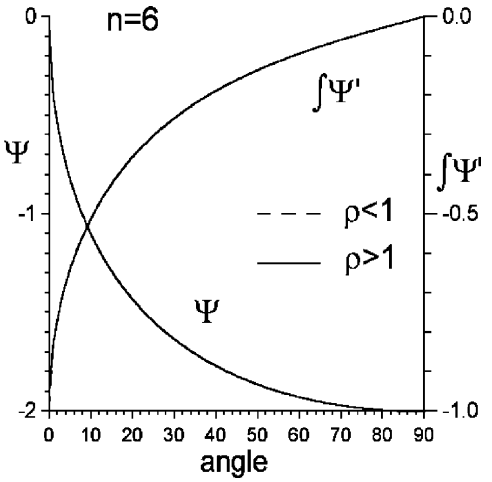

Fig. 14. Ψ and $\int\Psi'\,d\phi$ versus ϕ for $n = 6$.

Eq. (A.3). Our values agree with Amazigo's except when $n \geqslant 30$. (Our calculated values of his term δ, listed too in his Table 1, also disagree with his values for $n \geqslant 30$.) Atkinson and Champion (1985) found by another method values of Q for $n \leqslant 5$. These agree with those of Amazigo.

The first coefficient $\overline{a}_1$ of Eq. (37) of the text is related to Q by

$$\overline{a}_1 = \frac{Q}{n} = mQ. \tag{A.8}$$

This relationship is demonstrated in Table 3 of Appendix C. Therefore, except when $n \geqslant 30$, the value of the J-integral that can be obtained from our analysis is the same that Amazigo found. When Amazigo's values for $n \geqslant 30$ are corrected they do agree.

Appendix B

A verification is made here that the inverse Cassini oval coordinate system (Moon and Spencer, 1971) shown in Fig. 4 gives contours of constant stress magnitude for the mode III crack. (These contours are shown in Figs. 1.13a, b of Weertman (1996) without recognition they are inverse Cassini ovals. They are shown in Fig. 4.3-1 of Unger (1995) with this recognition, along with a different proof they are stress magnitude contours.)

The coordinate system of Fig. 3 (in normalized units in which $a = 1$) is given by (Weertman, 2000)

$$z = x + \mathrm{i}y = \sqrt{1 + w^2} = \sqrt{1 + (u + \mathrm{i}v)^2}. \tag{B.1}$$

The finger and thumb differentials (Weertman, 2000) of the coordinate system are $\partial/\partial F = \Gamma\partial/\partial u$ and $\partial/\partial T = \Gamma\partial/\partial v$, (on noting that $\delta F = \delta u\sqrt{(\partial x/\partial u)^2 + (\partial y/\partial u)^2}$ and $\delta T = \delta v\sqrt{(\partial x/\partial v)^2 + (\partial y/\partial v)^2}$) where the metric Γ is given by

$$\Gamma^2 = \frac{1}{z'\overline{z}'} = \frac{\sqrt{(1 + w^2)(1 + \overline{w}^2)}}{w\overline{w}} = \frac{\sqrt{(u^2 - v^2 + 1)^2 + 4u^2v^2}}{u^2 + v^2}, \tag{B.2}$$

and $z' = \mathrm{d}z/\mathrm{d}w$, $\overline{z}' = \mathrm{d}\overline{z}/\mathrm{d}\overline{w}$. (The angle ψ of the tangent to a finger trajectory is given by $\tan\psi = -\mathrm{i}(z' - \overline{z}')/(z' + \overline{z}')$.) In Fig. 3 coordinate system the stress components are (when $\sigma_A = 1$)

$$\sigma_{TZ} \equiv \varsigma_F = \varsigma = \Gamma(= \text{stress magnitude}), \quad \sigma_{ZF} \equiv \varsigma_T = 0. \tag{B.3}$$

Along a constant stress contour of Fig. 4 Γ is a constant. (Note that Γ is not a constant along the finger or thumb trajectories of Fig. 3 in which either u or v is held constant.) Now change to the inverse Cassini oval coordinate system with variables s and t:

$$z = x + \mathrm{i}y = \sqrt{1 + w^2} = \frac{1}{\sqrt{1 + \exp 2\overline{q}}} = \frac{1}{\sqrt{1 + \exp 2(s - \mathrm{i}t)}}. \tag{B.4}$$

Eq. (B.2) becomes

$$\Gamma^2 = \varsigma^2 = \frac{\sqrt{(1 + w^2)(1 + \overline{w}^2)}}{w\overline{w}} = \exp[-(q + \overline{q})] = \exp(-2s). \tag{B.5}$$

Note that $\Gamma = \varsigma$ remains constant when s is held constant and t is varied. Thus the inverse Cassini oval coordinate system gives constant stress contours.

Appendix C

The values of the constants $\beta_0, \beta_2, \beta_4, \ldots$ are listed in Table 1. See Tables 2–4.

Table 1
Beta constants

m	β_0	β_2	β_4	β_6	β_8	β_{10}
1	1	0	0	0	0	0
0.8	1.0045	−0.00040359	−0.00001820	−0.00000815	−0.00000730	−0.00000360
0.4	1.0735	−0.00659825	−0.00006005	0.00002852	0.00001050	0.00000167
0.2	1.2184	−0.02308512	0.00023139	0.00044616	0.00032424	0.00014109
0.1	1.44	−0.06484964	−0.00117698	0.00031102	0.00022031	0.00008085
0.05	1.736	−0.14725855	−0.00645528	−0.00087101	−0.00052370	−0.00026977
0.025	2.055	−0.25494269	−0.01118927	0.00123175	0.00212553	0.00105995
0.01	2.63	−0.50094515	−0.04264187	−0.00480160	0.00128860	0.00114142
0.005	3.28	−0.81029898	−0.10351820	−0.02757797	−0.0194616	−0.00392626

Table 2
$\Delta\Omega^{>}$, $\Delta\Omega^{<}$ at various ϕ for $m = 1/5$

$\Delta\Omega^{<}$	$\Delta\Omega^{>}$	ϕ	$\Delta\Omega^{<}$	$\Delta\Omega^{>}$	ϕ
−1.7921	−1.7921	0	−0.3721	−0.3719	47.25
−1.5457	−1.5460	2.25	−0.3351	−0.3350	49.5
−1.4366	−1.4366	4.5	−0.2999	−0.2998	51.75
−1.3482	−1.3479	6.75	−0.2665	−0.2665	54
−1.2699	−1.2694	9	−0.2349	−0.2350	56.25
−1.1980	−1.1975	11.25	−0.2052	−0.2053	58.5
−1.1304	−1.1300	13.5	−0.1774	−0.1775	60.75
−1.0661	−1.0659	15.75	−0.1515	−0.1516	63
−1.0045	−1.0045	18	−0.1276	−0.1277	65.25
−0.9453	−0.9455	20.25	−0.1057	−0.1058	67.5
−0.8881	−0.8884	22.5	−0.08580	−0.08583	69.75
−0.8328	−0.8332	24.75	−0.06792	−0.06792	72
−0.7794	−0.7798	27	−0.05210	−0.05207	74.25
−0.7276	−0.7279	29.25	−0.03834	−0.03830	76.5
−0.6775	−0.6777	31.5	−0.02664	−0.02662	78.75
−0.6290	−0.6291	33.75	−0.01709	−0.01705	81
−0.5821	−0.5821	36	−0.009621	−0.009659	83.25
−0.5368	−0.5367	38.25	−0.004279	−0.004265	85.5
−0.4932	−0.4930	40.5	−0.001070	−0.001066	87.75
−0.4511	−0.4509	42.75	0	0	90
−0.4108	−0.4105	45			

Table 3
$\bar{a}_1$, $\bar{a}_2$ and $m|Q|$ for different m

m	1	4/5	2/5	1/5	1/10	1/20	1/40	1/100	1/200
$\bar{a}_2$	0.5	0.50185	0.51015	0.58611	0.65515	0.72074	0.77256	0.81046	0.82970
$\bar{a}_1$	0.5	0.49810	0.46886	0.41015	0.33533	0.25950	0.19195	0.12538	0.09125
$m\|Q\|$	0.5	0.49809	0.46881	0.41013	0.33497	0.25840	0.19162	0.12482	0.08914

Table 4
$|Q_{\mathrm{Amaz}}|$ and $|Q|$ for different $n = 1/m$

n	1	1.5	2	3	5	10	20	30	50	100
$\lvert Q_{\mathrm{Amaz}}\rvert$	0.5	0.74061	0.96380	1.3674	2.0507	3.3497	5.16814	8.5420	12.359	39.825
$\lvert Q\rvert$	0.5	0.74060	0.96381	1.3674	2.0507	3.3497	5.16816	6.5312	8.6536	12.482

Appendix D

Because summation terms containing cosine functions do not change sign at $\phi = 0$ the convergence of the summation can be very slow. This appendix describes summation tricks at $\phi = 0$ (and $\varsigma = \varsigma_A$) used in the evaluation of $\overline{u}^{>}$ and $\Omega^{<}$ to solve this problem. It also discusses the summation trick used to obtain $\partial\overline{u}/\partial\varsigma$ at small values of ϕ.

At $\phi = 0$ (and $\varsigma = \varsigma_A$) the potential $\overline{u}_0^{>}$ is equal to (see Eq. (45))

$$\frac{\overline{u}_0^{>}}{a\varsigma_A} = 1 + (\beta_0 - 2)a_1 - \beta_0 \sum_{N=1}^{\infty} a_{2N+1}. \tag{D.1}$$

Since $\sum_{N=0}^{\infty} a_{2N+1} = 1$ there is no need to evaluate $\overline{u}_0^{>}$ by summation in Eqs. (45) and (D.1) at $\phi = 0$. Note too that since $\widetilde{a}_{2N+1}^{2K}$, given by Eq. (48), decreases as $1/(2N+1)^2$ the summation for $\overline{u}_{2K}^{>}$ at $\phi = 0$ and $\varsigma = \varsigma_A$ converges rapidly. Thus $\overline{u}^{>}$ easily is evaluated accurately at $\phi = 0$.

From Eq. (42) $\Omega_0^{<}$ is equal to (at $\phi = 0$ and $\varsigma = \varsigma_A$)

$$\Omega_0^{<} = a\varsigma_A\beta_0 \sum_{N=1}^{\infty} b_{2N}\sqrt{1 + \frac{(1-m)^2}{4m(2N)^2}}\{\cos N\pi - 1\}. \tag{D.2}$$

The $\cos N\pi$ term causes no problem in the summation because it alternates in sign. The term 1 does because it does not alternate in sign. Let

$$\sum_{N=1}^{\infty} b_{2N}\sqrt{1 + \frac{(1-m)^2}{4m(2N)^2}} = \sum_{N=1}^{\infty} b_{2N} + \sum_{N=1}^{\infty} b_{2N}\left\{\sqrt{1 + \frac{(1-m)^2}{4m(2N)^2}} - 1\right\}. \tag{D.3}$$

Note that $\sum_{N=0}^{\infty} b_{2N} = 1$ and, at large values of N, that $\sqrt{1 + (1-m)^2/4m(2N)^2} - 1 \approx (1-m)^2/8m(2N)^2$. The second summation on the right-hand side of Eq. (D.3) converges rapidly and the first summation has a known value. Thus $\Omega_0^{<}$ is easily evaluated at $\phi = 0$. There are only five $\Omega_{2K}^{<}$ used in the paper. Thus $\Omega^{<}$ is accurately found at $\phi = 0$.

One of the summation that causes problems in evaluating $\partial\overline{u}/\partial\varsigma$ accurately (see Eq. (39)) is

$$\sum_{N=1}^{\infty} \overline{a}_{2N}\left\{\frac{1}{2}\sqrt{\left(1 - \frac{1}{m}\right)^2 + \frac{4}{m}(2N)^2}\right\}\sin(2N)\phi. \tag{D.4}$$

(The other troublesome summation is the one with $\cos(2N+1)\phi$ terms in Eq. (40).) At large values of N

$$\begin{aligned}\sqrt{\left(1 - \frac{1}{m}\right)^2 + \frac{4}{m}(2N)^2} &= \frac{2}{\sqrt{m}}(2N) + \sqrt{\left(1 - \frac{1}{m}\right)^2 + \frac{4}{m}(2N)^2} - \frac{2}{\sqrt{m}}(2N) \\ &\approx \frac{2}{\sqrt{m}}(2N) + \frac{\sqrt{m}}{4}\left(1 - \frac{1}{m}\right)^2 \Big/ (2N).\end{aligned} \tag{D.5}$$

Note that the summation $\sum_{N=1}^{\infty} b_{2N}(2N)\sin(2N)\phi$ can be found directly, without the need of a summation, by differentiating $\overline{u}$ given by Eq. (15). Similarly, $\sum_{N=0}^{\infty} a_{2N+1}(2N+1)\cos(2N+1)\phi$ also is found by the same differentiation.

References

Amazigo, J.C., 1974. Fully plastic crack in an infinite body under anti-plane shear. International Journal of Solids and Structures 10, 1003–1015.

Amazigo, J.C., 1975. Fully plastic center cracked strip C under anti-plane shear. International Journal of Solids and Structures 11, 1291–1299.

Atkinson, C., Champion, C.R., 1985. A boundary integral equation formulation for problems involving non-linear power-law materials. IMA Journal of Applied Mathematics 35, 23–38.

Moon, P., Spencer, D.E., 1971. Field Theory Handbook Including Coordinate Systems, Differential Equations and their Solutions, second ed. Springer-Verlag, Berlin.

Rice, J.R., 1968. Mathematical analysis in the mechanics of fracture. In: Liebowitz, H. (Ed.), Fracture, An Advanced Treatise, vol. II. Academic Press, New York, pp. 191–311.

Thomson, R., 1978. Brittle fracture in a ductile material with application to hydrogen embrittlement. Journal of Materials Science 13, 128–142.

Unger, D.J., 1995. Analytical Fracture Mechanics. Academic Press, San Diego, CA.

Weertman, J., 1978. Fracture mechanics: a unified view for Griffith–Irwin–Orowan cracks. Acta Metallurgica 26, 1731–1738.

Weertman, J., 1991. Crack tip plastic zone, dislocation crack tip shielding, and the dislocation crack extension force. In: Liaw, P.K., Marcus, H.L., Santner, J.S., Weertman, J.R. (Eds.), Morris E. Fine Symposium. Minerals, Metals & Materials Society of the AIME, Warrendale, PA, pp. 339–347.

Weertman, J., 1996. Dislocation Based Fracture Mechanics. World Scientific Publishing Company, Singapore.

Weertman, J., 2000. Application of curvilinear coordinates to dislocation density fields around cracks in linear elastic–plastic solids. Materials Science and Engineering. A Structural Materials, Properties, Microstructure and Processing 285A, 380–390, Erratum 2000, 293A, 297.

Weertman, J., 2001. Curvilinear coordinates for mode III crack plastic zone in work hardening solid. Materials Science and Engineering. A Structural Materials, Properties, Microstructure and Processing 314A, 100–107.